ELSEVIER

Coordination Chemistry Reviews
190–192 (1999) 1003–1022

COORDINATION CHEMISTRY REVIEWS

www.elsevier.com/locate/ccr

Studies of hyperfine interactions in [2Fe–2S] proteins by EPR and double resonance spectroscopy

Richard Cammack *, Elaine Gay, Jas K. Shergill

Centre for the Study of Metals in Biology and Medicine, Division of Life Sciences, King's College, London W8 7AH, UK

Contents

Abbreviations: c.w., Continuous-wave; r.f., Radiofrequency; EPR, Electron paramagnetic resonance; ENDOR, Electron nuclear double resonance; ESEEM, Electron spin–echo envelope modulation; NMR, Nuclear magnetic resonance.

* Corresponding author. Fax: +44-171-3334500.
E-mail address: richard.cammack@kcl.ac.uk (R. Cammack)

PII: S0010-8545(99)00155-1

Abstract

We review the measurement of nuclear hyperfine interactions in the reduced [2Fe–2S] proteins, and the information on molecular and electronic structure of the clusters that can be derived from them. Several major types of cluster-binding domains can be distinguished: (1) the structurally well-characterized proteins typified by ferredoxins from plant-type photosynthesis and cytochrome P-450 monooxygenases; (2) a type of cluster found in molybdenum hydroxylases such as xanthine oxidase; (3) the structurally uncharacterized [2Fe–2S] ferredoxins from nitrogen-fixing bacteria; (4) the Rieske proteins of respiratory and photosynthetic electron-transfer chains, and similar clusters in nonheme iron oxygenases. All have cysteine ligands to the cluster, but in Rieske proteins two are replaced by histidine nitrogen ligands. The interactions with ^{1}H and ^{14}N of the protein depend on the folding of the polypeptide chain around the clusters. A range of methods is available to measure interactions with these and other nuclei, including continuous-wave and pulsed ENDOR, and electron spin–echo envelope modulation in pulsed EPR (ESEEM). Couplings to the β-CH_2 and possibly the α-CH protons are observable in the ENDOR spectra in the frequency range 1–15 MHz. Couplings to ^{14}N can also be observed and, by means of their quadrupole coupling, identified as polypeptide nitrogens and histidine imidazole nitrogens. The methods are complementary to other structural techniques in that they can measure the spin density distribution on the clusters, and proton exchange reactions with $^{2}H_2O$. Orientation-selective measurements provide structural information without the need for crystals, and so have the potential to observe changes to the cluster environment induced by amino-acid substitutions, and transient intermediates which are trapped by freezing.

Keywords: Electron paramagnetic resonance; Electron nuclear double resonance; Ferredoxin; Iron–sulfur protein

1. Introduction

Iron–sulfur proteins are widespread in biochemistry, and have numerous functions, most frequently in electron transport [1–3]. In these proteins, the iron–sulfur clusters comprise iron atoms, bridged by sulfides, and bound directly to side-chains, which are usually cysteines but occasionally histidine or other amino acids. There are different types of iron–sulfur clusters, classified as [2Fe–2S], [3Fe–4S], [4Fe–4S], mixed-metal and hybrid types. The clusters are found both in simple iron-sulfur proteins (ferredoxins), and in more complex enzymes. In the early EPR spectroscopic studies of the iron–sulfur proteins, hyperfine interactions to various isotopes in the clusters played a part in determining their structure and composition. This was comprehensively reviewed in Coordination Chemistry Reviews by Tsibris and Woody [4]. Here we present an overview of subsequent work on the [2Fe–2S] clusters by methods based on EPR spectroscopy, and the potential for these methods in the future.

The coordination of the different types of [2Fe–2S] clusters is illustrated in Fig. 1. The structures of the proteins have been determined by X-ray crystallography [5–9] and NMR [10–12] and they show that some backbone amide nitrogens are within hydrogen-bonding distance of the sulfurs of the cluster. Contact shifts, equivalent to 150 MHz, are observed in the NMR spectra [13,14].

In some [2Fe–2S] proteins one of the cysteines is substituted by another amino acid residue such as serine or aspartate [15]. More substitutions have been engineered by site-directed mutagenesis, and in some cases they appear to function correctly, but in other cases the cluster is not inserted (reviewed in Ref. [16]). An example where substitutions have been successful is fumarate reductase of *Escherichia coli* [17].

2. [2Fe–2S] proteins

The proteins with [2Fe–2S] clusters, which are the subject of this review, may be classified in various ways. Proteins with similar structure and function have been isolated from animals, plants, and bacteria. Probably the most useful classification for our purposes is based on the overall fold of the protein around the cluster, which depends on the positions of the ligating amino acids, cysteines or histidines in the protein sequence. Other amino acids around the cluster may vary considerably, and proteins with similar folding patterns may be very different in their overall sequence.

Each of the different types of [2Fe–2S] cluster-binding motifs has been shown to occur in enzymes as well as simple ferredoxins. Therefore they can be considered as

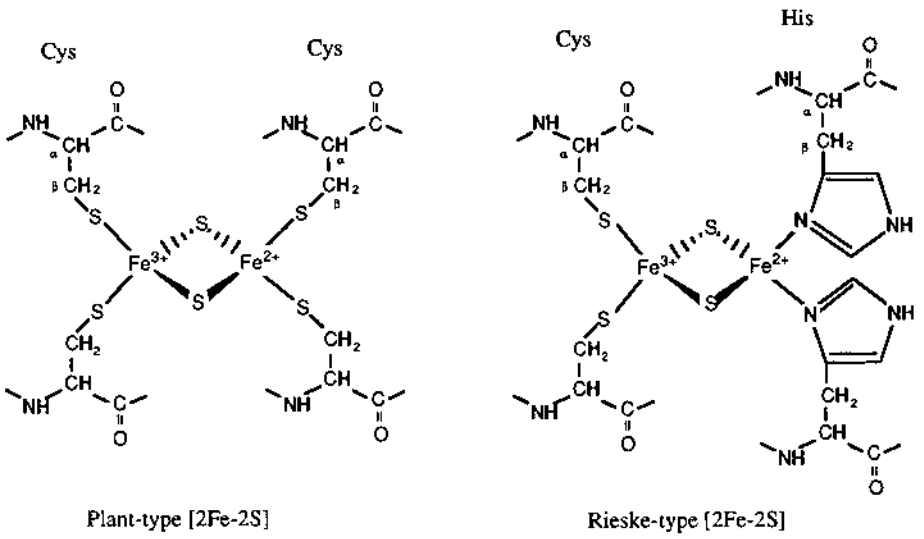

Fig. 1. Covalent structures of the different types of [2Fe–2S] clusters.

domains of more complex electron-transfer sequences. They are of particular importance in the energy-conserving electron-transfer chains of respiration and photosynthesis.

2.1. Plant-type

The name 'ferredoxin' was first given to a protein from the fermentative bacterium *Clostridium pasteurianum* by Mortenson et al. [18], which proved to be a 2[4Fe–4S] protein. By extension the name was applied by Tagawa and Arnon [19] to a red-coloured [2Fe–2S] protein involved in photosynthesis of spinach chloroplasts. Ferredoxins are now defined as iron–sulfur proteins for which the sole function is electron transport. Proteins similar to plant ferredoxin have been isolated from cyanobacteria, which also use oxygen-evolving photosynthesis. Soon after the isolation of spinach ferredoxin, proteins containing similar clusters were isolated from animal adrenal glands, and a strain of *Pseudomonas putida*, both of which acted as electron donors to P-450-type monooxygenases, and were given the trivial names adrenodoxin and putidaredoxin. Proteins like adrenodoxin have been found in many animal tissues, not just adrenal glands, and are sometimes described as 'vertebrate-type', although similar proteins have been found in microorganisms. All of these proteins have similar arrangements of cysteines in their amino-acid sequences, which is folded in a similar way around the cluster. For present purposes, and for historical reasons, we will refer to them as 'plant-type'.

All the [2Fe–2S] ferredoxins are paramagnetic in their reduced states. The EPR spectra of the ferredoxins from plants and cyanobacteria are rhombic in shape ($g_x \neq g_y \neq g_z$), while those of the ferredoxins such as adrenodoxin and putidaredoxin are more axial in form ($g_x \approx g_y \neq g_z$), and have narrower linewidths.

More complex iron–sulfur proteins have been found to contain domains that are similar to the ferredoxins. An example is phthalate dioxygenase reductase from the bacterium *Burkholderia* (formerly *Pseudomonas*) *cepacea*, which comprises an iron–sulfur protein domain similar to plant ferredoxin, and a flavoprotein domain similar to plant ferredoxin:NADP reductase [20]. Succinate dehydrogenase (Complex II) of the respiratory chain, and its anaerobic counterpart, fumarate reductase, also have a domain which is homologous to the [2Fe–2S] ferredoxins [21,22].

2.2. Xanthine-oxidase type

The molybdenum hydroxylases, of which xanthine oxidase is probably the best-known example, contain two [2Fe–2S] clusters [23]. Two different EPR signals are observed in these proteins, one with unusually high rhombicity [23]. The aldehyde oxidoreductase of *Desulfovibrio gigas* is in this class [24]. Its structure reveals one [2Fe–2S] cluster-binding domain similar to the plant-type ferredoxin, and one with a different fold. The latter will be referred to here as 'xanthine-oxidase type'.

2.3. Clostridial-type

An iron–sulfur protein was isolated from *C. pasteurianum* [25,26], and from other nitrogen-fixing bacteria. These proteins were also paramagnetic in the reduced state and proved to have similar [2Fe–2S] clusters. The amino acid sequence of the *C. pasteurianum* protein shows a different pattern of cysteine residues from the plant and P-450 types [27]. The structure of these proteins has not been determined and most of the structural information has been derived from spectroscopic techniques such as EPR, ENDOR and resonance Raman spectroscopy [28,29].

2.4. Rieske-type

A distinct type of [2Fe–2S] protein was observed in the bc_1 complex (ubiquinol:cytochrome *c* reductase, Complex III) of the mitochondrial respiratory chain by Rieske et al. [30] and became known as the Rieske protein. Its EPR signal was characterized by low *g*-factors and large anisotropy, and proteins of this type had unusually positive reduction potentials. Spectroscopic studies indicated that it had two out of four non-cysteine ligands, which were shown by ENDOR spectroscopy to be histidine nitrogens [31,32]. This was confirmed by ESEEM [33], and later by crystallography [34].

[2Fe–2S] clusters with similar EPR signals to the Rieske protein were observed in nonheme iron-containing hydroxylases such as benzene, naphthalene and phthalate dioxygenase [35–37], and were shown to have similar structures [8]. The clusters have more negative reduction potentials than the Rieske protein, but otherwise appear to be structurally similar.

3. Information derived from hyperfine and quadrupolar coupling

ENDOR and pulsed EPR, which are described in more detail later, are techniques for precise measurement of nuclear hyperfine and quadrupolar interactions. There are two components to the hyperfine interaction:

The *dipolar interaction* is equivalent to the interaction through space between two bar magnets. The dipolar coupling is anisotropic. According to the point-dipole formulation, the strength of the interaction varies as $(1 - 3\cos^2\theta)/r^3$, where r is the distance between the electron and nucleus and θ is the angle between the inter-spin vector and the applied magnetic field. Thus the dipolar interaction depends on the relative positions, in polar coordinates, of the nuclear spin relative to the paramagnetic centre. For iron–sulfur clusters this is only an approximation, however, since the electron density is significantly delocalized over the sulfur ligands and other atoms.

The *Fermi contact* or *exchange interaction* operates through electron orbitals. Electrons in the *s* orbitals have a finite electron density at the nucleus; other electrons, for example in π orbitals, are coupled through exchange interactions with s electrons, a process known as *core polarization*. The contact interaction is

isotropic, to first order, and is also responsible for contact shifts in NMR of paramagnetic centres. The strength of the exchange interaction depends on the type and number of intervening bonds between the nuclear spin and the paramagnet. Moreover it depends on the bond angles, in a similar way to the Karplus relationship in NMR spectroscopy [14].

For nuclei with $I > 1/2$ such as ^{14}N, the nuclear quadrupolar interaction may be observed both in ENDOR and ESEEM. The quadrupole coupling e^2qQ/h and the asymmetry parameter η for a nucleus are indicators of the electric-field gradient around the nucleus, and thus its chemical state. In iron–sulfur proteins, it is possible to discriminate between the amide nitrogens of the polypeptide backbone, and imidazole nitrogens from the amino acid histidine.

Changes in the protein conformation around the active site can be induced, for example by binding of a substrate to an enzyme, or site-directed mutagenesis. These can cause changes in the pattern of hyperfine couplings, which are not observed in the EPR spectrum. ^{14}N couplings as observed in ESEEM are normally only seen to change in response to relatively drastic conformational changes. On the other hand proton couplings are particularly sensitive to such changes, giving changes in the ENDOR spectrum which are readily detected but difficult to interpret. In order to determine the nature of the conformational change, it is necessary to re-identify the protons giving rise to the individual couplings, and obtain positional information.

4. EPR spectroscopy

In EPR, hyperfine splittings are only resolved if they are at least comparable in magnitude with the inhomogeneously-broadened linewidth. This confines the method to couplings to nuclei of the iron–sulfur cluster itself. Couplings to the iron and bridging sulfides were observed in the EPR spectra of ^{57}Fe-enriched and ^{33}S-enriched ferredoxins, and proteins in which the bridging sulfides were substituted by ^{77}Se (reviewed by Tsibris and Woody [4]). The iron and sulfur can readily be replaced by denaturation of the protein and reconstitution with iron and inorganic sulfide [38]. An example is the hyperfine splitting due to ^{57}Fe (Fig. 2). On the low-field $g_{\|}$ feature, a clear 1:2:1 splitting is observed, indicating hyperfine interaction with two iron nuclei ($I = 1/2$). Similar splittings were observed in ferredoxins in which the bridging sulfides were substituted with ^{77}Se ($I = 1/2$). These results confirmed the [2Fe–2S] stoichiometry of the clusters.

In EPR a major contribution to the line width is the effects of random strains on the protein structure, induced by freezing [39,40] This also contributes to line broadening of the ENDOR spectrum through the anisotropy of the hyperfine interaction.

Hyperfine couplings to these directly-coupled nuclear spins may be extracted from the EPR spectra by computer simulation. This provides an estimate of the parameters of the electron g-matrix and the hyperfine coupling matrix, A.

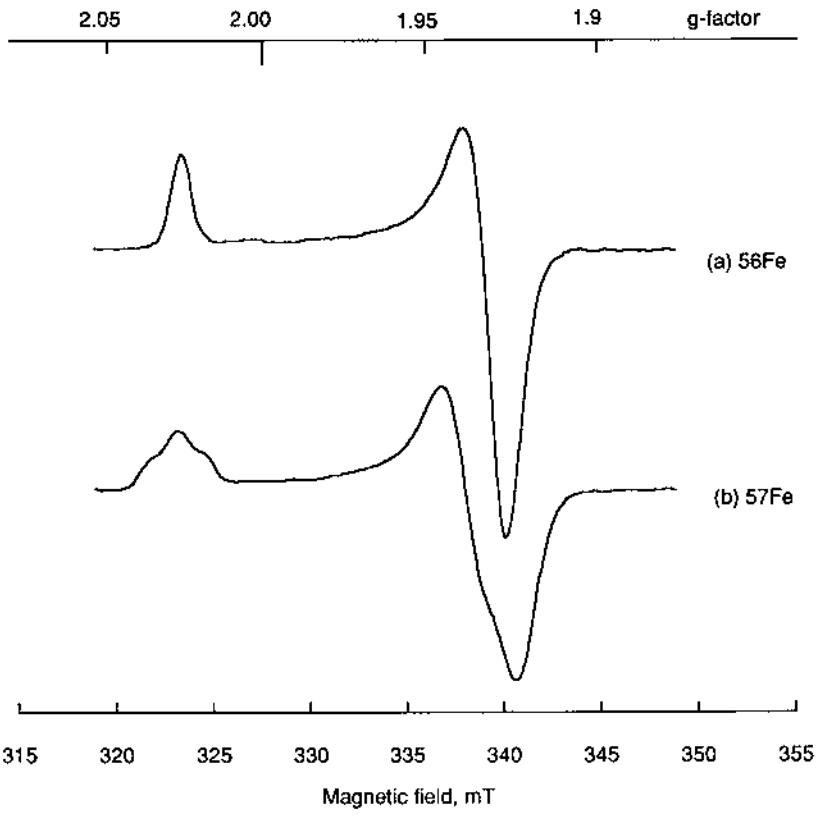

Fig. 2. EPR spectra of reduced adrenal ferredoxin, recorded at 77 K; (a) native protein; (b) reconstituted with ^{57}Fe.

5. ENDOR

Electron-nuclear double resonance is a technique that was devised by Feher [41] to measure electron-nuclear hyperfine couplings, a, by applying a combination of microwave radiation at the electron resonant frequency, and radiofrequency (r.f.) at nuclear resonant frequencies. For a given EPR resonance it provides a spectrum of nuclei interacting with the unpaired electrons in the paramagnetic site. Applications to transition-metal proteins have been described by Hüttermann and Kappl [42], Hüttermann [43,44], Hoffman [45] and Lowe [46]. ENDOR measurements may be divided into two types, continuous-wave and pulsed, corresponding with the two types of EPR experiment.

In a typical continuous-wave ENDOR experiment, the microwave frequency and the applied magnetic field, B_0, are fixed to observe a specific feature in the EPR spectrum. The temperature and the microwave power are adjusted so that the EPR spectrum is saturated, and thus, its amplitude is decreased. Under these conditions, electron-spin relaxation is a limiting factor for the signal amplitude. The sample is

irradiated with a sweep of radiofrequency (r.f.) energy to excite nuclear-spin transitions. When the r.f. field is in resonance with a transition of a nucleus which is magnetically coupled to the paramagnet, an increase in the EPR amplitude is recorded.

Various processes give rise to the ENDOR phenomenon. Saturation is alleviated by redistribution of the electron spin populations, and also by enhancement of electron-spin relaxation pathways. There is a third type of process known as distant ENDOR, which involves spin diffusion and is due to the cumulative effect of many nuclei at distances which are too great to give a significant splitting of the spectrum.

An advantage of ENDOR is that the linewidth is much narrower than in EPR (typically less than 0.5 MHz in the solid state) and so analysis of the observed ENDOR frequencies gives hyperfine coupling constants, which are often unresolved in EPR of the solid state. Also, ENDOR can resolve coupling due to multiple nuclei, which in EPR would produce a multitude of lines and be difficult to resolve. ENDOR also allows the precise determination of hyperfine coupling (a-values).

In ENDOR spectra, information is mainly derived from the positions of the resonances, which define the hyperfine coupling. The amplitudes of the resonances are more difficult to interpret, since they depend on complex relaxation pathways which are susceptible to various influences. For a paramagnet in a crystal or in solution, each hyperfine coupling contributes a pair of lines to the ENDOR spectrum. The interpretation of the line positions depends on the values of ν_n ($=\mu_N B_0$), the nuclear Larmor frequency and a, the hyperfine coupling constant. In the case where $\nu_n > a/2$, as is usual for protons, the two lines will be centred at ν_n and separated by a. In the case where $a/2 > \nu_n$, as in the case of strong coupling to other nuclei, the lines are centred at $a/2$ and separated by $2\nu_n$. The distant ENDOR effect gives rise to a matrix line at the nuclear Larmor frequency.

In spectra of proteins at X-band frequency, 9.5 GHz, overlap of multiple ENDOR lines due to protons can obscure the effect of coupling to other nuclear spins such as ^{14}N. Ambiguities may be resolved by operating at Q-band frequency, 35 GHz [45], which has the effect of separating the proton lines from the rest of the spectrum.

In the solid state, g and A are anisotropic, and their principal axes are not necessarily colinear. Hence the line shapes are complex. The EPR spectrum derives from a statistical distribution of molecules with different orientations relative to the applied field. ENDOR spectra recorded at the ends of the EPR spectrum correspond to specific orientations (B_0 aligned with g_x and g_z) [47]. This is the principle of *orientation selection*. By analysis of ENDOR spectra recorded at the extreme and intermediate positions, it is possible to determine the axes of the g-matrix relative to the molecular structure by computer simulation [48–51]. This can be used to derive structural information from frozen solutions of metalloproteins for which it is usually impossible to obtain sufficiently large single crystals.

A number of different instrumental configurations are used for ENDOR spectroscopy [52]. The Bruker broadband ENDOR spectrometer uses radiofrequency modulation and provides a first-derivative presentation of hyperfine couplings. Multiple proton hyperfine coupling may be resolved in the spectra (Fig. 3). The

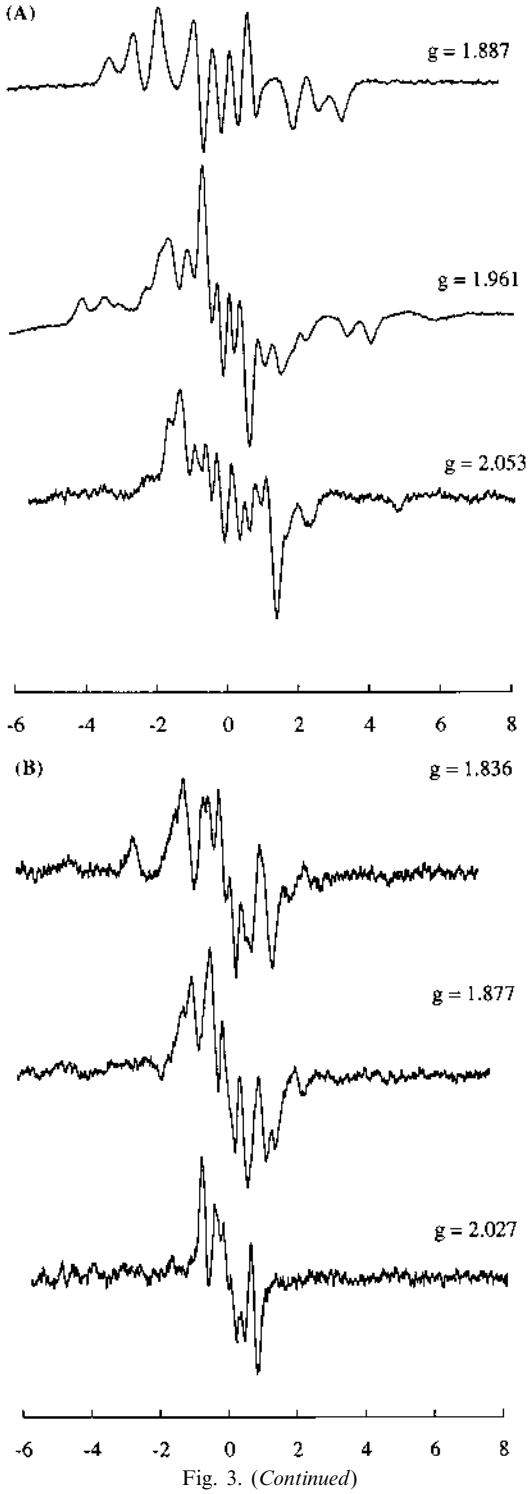

Fig. 3. (*Continued*)

Q-band spectrometer constructed by Hoffman's group [45] uses magnetic field modulation and records the spectrum in dispersion mode, giving a spectrum in which the hyperfine lines appear with the shape of absorption lines. This arrangement appears to be optimum for measurement of strong coupling.

5.1. Applications of ENDOR

5.1.1. ^{57}Fe

The ENDOR and Mössbauer spectra of a variety of ^{57}Fe-enriched [2Fe–2S] ferredoxins were analyzed by Dunham et al., in their classic analysis of the spectroscopic parameters of the [2Fe–2S] proteins [53]. The anisotropy of the hyperfine interaction was determined by computer analysis of the ^{57}Fe hyperfine coupling at different g-factors. Combined with the hyperfine interactions observed in the Mössbauer spectra [54,55], magnetic susceptibility [56] and NMR contact shifts [57], it was possible to determine that the two iron atoms had hyperfine fields of opposite sign. These experiments confirmed the antiferromagnetically coupled model for the [2Fe–2S] clusters, proposed by Gibson et al. [58,59].

5.1.2. ^{1}H

Proton hyperfine coupling to the reduced [2Fe–2S] ferredoxins were first observed by Fritz et al. [39] and Bowman et al. [60]. The strongest coupling is expected to be to β-CH_2 protons of the cysteines coupled to the ferric iron [39]. ENDOR spectra of cyanobacterial ferredoxin grown on $^{2}H_2O$ medium, and therefore containing only ^{2}H at all positions in the amino acids were, as expected, devoid of proton resonances [61], which simplified the observation of ^{57}Fe coupling. When the protein was transferred to $^{1}H_2O$, weakly-coupled protons ($a \leq 5$MHz) were observed, but no exchangeable, strongly-coupled protons were observed. Some of the protons exchanged very slowly unless the cluster was destroyed and reconstituted. These early results are complementary to subsequent investigations of proton exchange using ESEEM and pulsed ENDOR [62,63] (see below).

C.w. ENDOR spectra of plant-type ferredoxins show couplings up to 12 MHz, with orientation dependence (Fig. 3). A number of studies have catalogued the hyperfine couplings in iron–sulfur proteins, which may be used as a 'fingerprint' for the cluster. At present the non-exchangeable protons have not been assigned to specific protons in the structure. The strongest coupling is expected to represent the β-CH_2 protons of the cysteine ligands to the Fe(III) atom (Fig. 1). The exchangeable protons are shown by subtle changes in the hyperfine pattern after transfer to

Fig. 3. Orientation dependence of the continuous-wave ENDOR spectra. (I) [2Fe–2S] ferredoxin from Arthrospira (formerly *Spirulina*) *platensis* ferredoxin, recorded at the three principal g-factors. Spectra were recorded in a Bruker broadband ENDOR spectrometer with the following conditions: temperature 15 K, microwave power 10 mW, microwave frequency 9.46 GHz. The frequency scale is presented in MHz relative to the proton Larmor frequency. (II) Rieske-type [2Fe–2S] ferredoxin from the benzene dioxygenase of *Pseudomonas putida* ML2, recorded at the three principal g-factors. Spectra were recorded at temperature 15 K, microwave power 10 mW, microwave frequency 9.45 GHz.

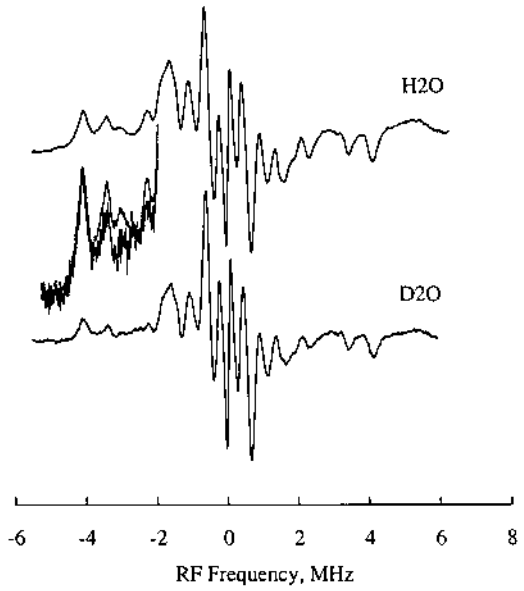

Fig. 4. Solvent-exchangeable protons in c.w. ENDOR spectra of *A. platensis* [2Fe–2S] ferredoxin.

$^{2}H_2O$ (Fig. 4). The exchangeable protons are likely to be NH protons within hydrogen bonding distance to sulfurs of the cluster, though the –OH of serine is also a possibility.

Normally ENDOR spectra are taken of purified proteins, but proton ENDOR spectra have been recorded from the Rieske clusters in membranes of heart mitochondria [64] and spinach chloroplasts [65] and the [2Fe–2S] clusters of succinate dehydrogenase of plant mitochondria [66]. This opens up the possibility of observing biochemical interactions of these complexes with quinones and other substrates, which cannot be observed in the isolated proteins.

^{1}H-ENDOR spectra have been recorded of the Rieske-type clusters in benzene dioxygenase and halobenzoate dioxygenase [65]. The strongest coupling, of the order of 11 MHz, is similar in magnitude to those observed in *A. platensis* ferredoxin.

5.1.3. ^{14}N

ENDOR spectra of the Rieske-type clusters provided definitive evidence for histidine ligands to the cluster [36]. In this case the ^{1}H and ^{14}N couplings overlap in the X-band ENDOR spectra, and so Hoffman and colleagues extended their investigations by using Q-band ENDOR spectroscopy. Gurbiel et al. [31] used orientation selection to assess the relative orientation of the planes of the histidine ligands to the Rieske iron–sulfur protein. A refined interpretation [67] yielded a structure in which the imidazole rings were orthogonal, which was subsequently confirmed by the crystallographic structure [34].

5.1.4. Other nuclei

Houseman et al. [68] observed low-frequency resonances at the ^{13}C and ^{15}N Larmor frequencies, in the Q-band ENDOR spectra of *Anabaena* ferredoxin. These were attributed to the isotopes present at natural abundance in the sample, being detected by the distant ENDOR effect. The ^{15}N coupling was further identified in samples enriched by growth in ^{15}N-containing medium.

6. Electron spin–echo envelope modulation (ESEEM)

The ESEEM effect, introduced by Mims [69] is a particularly sensitive method for observing weak anisotropic hyperfine and quadrupolar interactions, with nuclei such as ^{14}N and ^{2}H. The principles of the method are discussed by Mims and Peisach [70] Dikanov and Tsetkov [71] and Goldfarb [72]. Unlike the continuous-wave EPR and ENDOR methods described above, it uses a spin–echo sequence in a pulsed EPR spectrometer. The spin–echo amplitude is followed as a function of the time interval between pulses, giving a time-domain spectrum. While the echo decays with time, because of spin–spin relaxation processes, the envelope of the decay is not smooth, but shows modulations. The modulation frequencies are derived from the modulation pattern by Fourier transformation, giving a frequency-domain spectrum. The modulation frequencies correspond to ENDOR frequencies of nuclei that are coupled to the electron spin. They are a function of the hyperfine (a), nuclear Zeeman (ν_n) and nuclear quadrupole (e^2qQ/h) frequencies. The requirement for these modulations to be observed is that the microwave pulse is short enough so that the bandwidth can span the range of nuclear frequencies. Thus instead of using a separate radiofrequency source to excite the nuclear transitions as in ENDOR, they are stimulated by the microwave pulse.

Optimal ESEEM spectra are obtained when there is exact or nearly exact cancellation of the nuclear Zeeman interaction, $\nu_n = |\, a/2 \,|$. This is a situation where ENDOR spectra are difficult to observe, and therefore the two methods are complementary. For weak hyperfine interactions with ^{14}N nuclei the ESEEM spectra are dominated by the quadrupole interaction. As with ENDOR, information is derived principally from the line positions, rather than their amplitudes. The echo amplitude is a sinusoidal function of the delay time, τ. More quantitative information is derived by recording spectra over a range of values of τ and taking the projection of the maximum amplitude for each resonance.

The hyperfine and quadrupole parameters of the coupling to ^{14}N can be determined from a simulation of the ESEEM spectrum using hamiltonian matrix diagonalization. Calculations of theoretical spectra have indicated a number of situations where the hyperfine and nuclear quadrupole parameters can be derived by approximate formulae [73,74]. In general the $\Delta m_i = 2$ (so-called 'double-quantum') transitions give relatively narrow lines, one for each of the two spin manifolds ($m_S = +1/2$ and $m_S = -1/2$). The single-quantum transitions ($\Delta m_i = 1$) only give narrow lines in the case of the spin manifold where ν_n and $a/2$ cancel, where three nuclear quadrupole frequencies (ν_o, ν_-, and the double-quantum frequency ν_+) can

be resolved. Otherwise the $\Delta m_i = 1$ transitions tend to be broadened out by anisotropy. Hence, for near-cancellation conditions, four resonant frequencies are observed (Fig. 5), three from the manifold of levels in which cancellation occurs, and the double-quantum transition of the other manifold. From these it is possible to estimate a, e^2qQ/h and η. In the case of larger hyperfine coupling, the double-quantum transitions dominate the spectrum. From the two double-quantum frequencies alone the value of η cannot be estimated with certainty, but values over the possible range (0–1) make only a minor uncertainty (about $\pm 15\%$) in the estimation of the coupling parameters [75].

Spectra are more complex when more than one nuclear interaction is involved, and it is necessary to identify the resonances from each nucleus. As with NMR, it

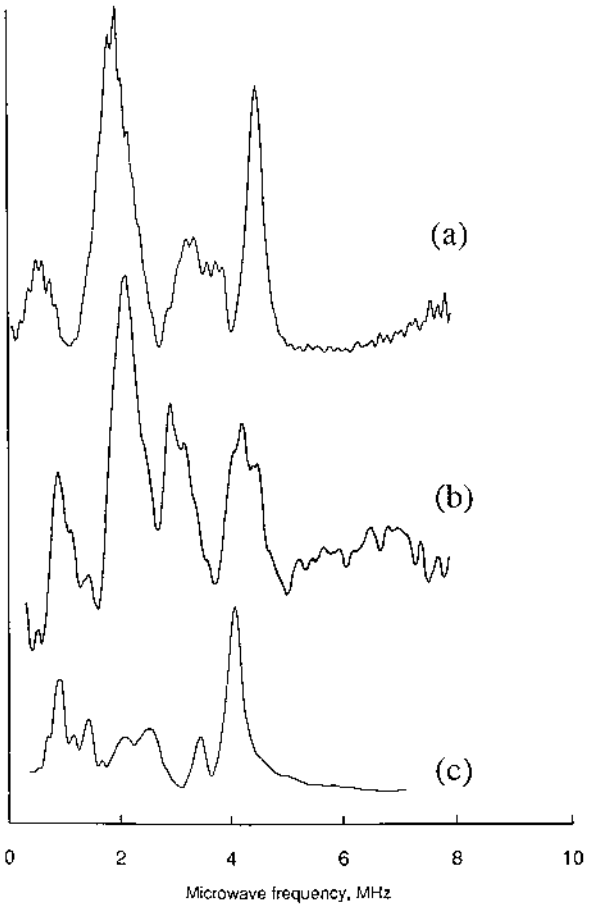

Fig. 5. Frequency-domain ESEEM spectra of (a) *A. platensis* ferredoxin; (b) [2Fe–2S] ferredoxin from *T. vaginalis* (A. Chapman, J. McCracken, J. Peisach, unpublished results); (c) *C. pasteurianum* [2Fe–2S] ferredoxin; (d) Rieske cluster in *P. putida* benzene dioxygenase. The spectra show the low-frequency region, corresponding to ^{14}N coupling.

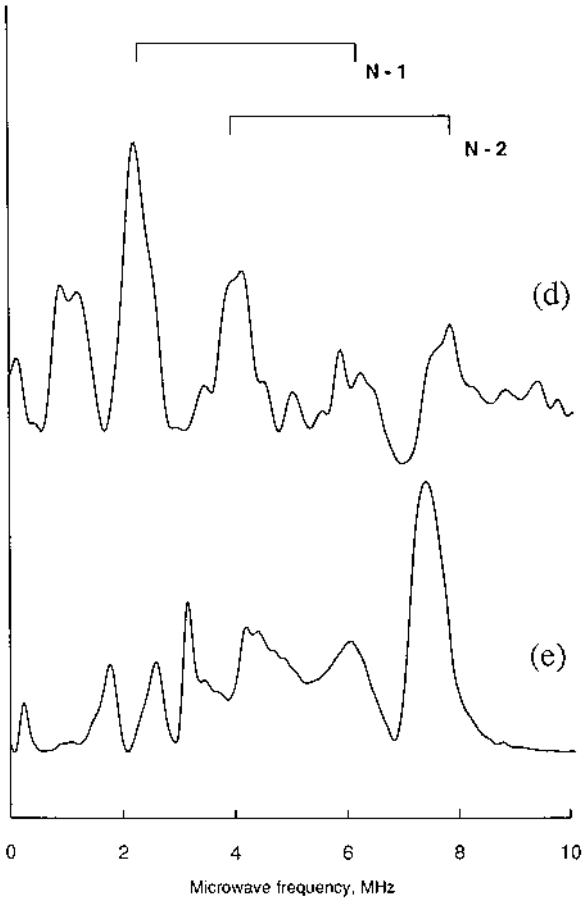

Fig. 5. (*Continued*)

is possible to correlate the peaks in pulsed EPR spectra by two-dimensional presentation of the data. The method of HYSCORE (hyperfine sublevel correlation spectroscopy) [25,76] is used to identify resonances which are correlated, i.e. derived from the same nuclear hyperfine interaction, and thus assign the spectra [77,78].

6.1. Applications of ESEEM

Time-domain ESEEM spectra of spinach ferredoxin, adrenodoxin and putidaredoxin were recorded by Peisach et al. [79]. The spectra were shown to be sensitive to exchange by ^{2}H, which gives strong modulations due to its quadrupole moment. Further studies used this effect to study the oxidation-state dependence of the rate of proton exchange at the cluster [62].

Hyperfine coupling to multiple protons gives lines distributed around the proton Larmor frequency as in ENDOR, but they are not so readily resolved. Dikanov

and Bowman presented a graphical method of resolving such resonances, and measured the isotropic couplings to β-CH_2 protons in the plant-type ferredoxin from *Porphyra umbilicalis*. From this, a Karplus-type analysis of the bond angles to the cluster was possible [80].

As shown in Fig. 5, ESEEM spectra of [2Fe–2S] clusters show well-resolved resonances from ^{14}N couplings (Table 1). For the plant-type, xanthine-oxidase and clostridial-type proteins the hyperfine couplings *a* are small, of the order of 1 MHz. The quadrupole coupling is approximately 3.3 MHz, corresponding to those of amide nitrogens [81]. Presumably these are peptide nitrogens, but the mechanism of coupling is not yet established. One explanation is that they represent the α-amide nitrogens of the ligating cysteine residues, as has been observed in copper proteins [82]. An alternative explanation is the NH–S hydrogen bonds that are known to occur in the plant-type ferredoxins from the polypeptide backbone to the bridging and terminal ligands to the cluster [83]. If so, the hydrogen bonds appear to be a consistent feature of all [2Fe–2S] proteins examined.

The weakly-coupled nitrogens in plant-type ferredoxin were further examined by orientation-selective measurements at C-band (≈ 7 GHz) [84]. At this frequency the ^{14}N hyperfine coupling is closer to exact cancellation. Coupling to two nitrogens was resolved, and assigned to peptide nitrogens situated near to the plane of the [2Fe–2S] cluster.

Table 1
^{14}N couplings in [2Fe–2S] proteins, observed by ESEEM

Protein	Method	Coupling constants (MHz)		Ref.
		a_{iso} [a]	e^2qQ/h	
Plant-type ferredoxin				
A. platensis ferredoxin	ESEEM	1.01	3.58	[99]
Porphyra umbilicalis	ESEEM	1.16, 0.4	3.26, 3.37	[84]
T. vaginalis	ESEEM	1.01	3.11	[a]
E. coli fumarate reductase	ESEEM	1.10	3.30	[83]
Arum maculatum succinate dehydrogenase	ESEEM	1.17		
C. pasteurianum [2Fe–2S] ferredoxin	ESEEM	0.61	3.30	[29]
C. pasteurianum Fd mutant C24A	ESEEM	0.82	3.08	[29]
Xanthine 0xidase cluster 1	ESEEM	0.6	3.3	[87]
cluster 2	ESEEM		3.3	
Rieske-type [2Fe–2S] clusters				
Bovine heart mitochondria	ESEEM	3.55, 5.2	2.25,	[64]
Spinach cytochrome b_6f complex	ESEEM	3.8, 4.6	2.9	[33]
Rhodobacter capsulatus complex III	ENDOR	4.5, 5.5	2.5–2.9, 2.5–2.9	[32]
B. cepacia phthalate dioxygenase	ENDOR	4.28, 5.49		[31]
P. putida benzene dioxygenase	HYSCORE	3.56, 4.78	2.60, 2.30	[77]
B. cepacia 2-halobenzoate 1,2-dioxygenase	ESEEM	3.8, 4.7	2.46, 2.33	[65]
B. cepacia 2,4,5-T monooxygenase	HYSCORE	4.0, 4.9	2–2.3, 3.6–4.1	[78]

[a] A. Chapman, R. Cammack, J. McCracken, J. Peisach, unpublished results.

Fig. 5(b) shows the ESEEM spectrum of the [2Fe–2S] ferredoxin from the protozoan *Trichomonas vaginalis*. This ferredoxin is unusual in being involved in electron transfer to hydrogenase, producing hydrogen [85]. It has recently been studied by NMR [86]. Despite the different function the ferredoxin shows an EPR spectrum similar to those of putidaredoxin and adrenodoxin, and this similarity is confirmed by the ESEEM spectrum (Fig. 5, Table 1).

ESEEM spectra recorded of xanthine oxidase [87], and the [2Fe–2S] ferredoxin from *C. pasteurianum* [29] showed weakly-coupled amide nitrogens similar to those found in plant-type ferredoxins. This implies that there are no directly-coupled nitrogen nuclei in these clusters, but NH–S hydrogen bonds are likely. Exchange into $^{2}H_2O$ showed that the clusters were readily accessible to solvent. In the case of *C. pasteurianum* only weak coupling to ^{14}N was detected, even in a mutant version of the protein having only three cysteines. The latter mutant presumably has a fourth oxygen-containing ligand to the cluster.

For Rieske-type clusters the imidazole nitrogens coordinated to the cluster have larger values of a and only the two double-quantum transitions are observed for each ^{14}N. Spectra have been recorded of the Rieske proteins in complexes isolated from mitochondria, chloroplasts and photosynthetic bacteria [33]. The estimates of coupling derived from these agree reasonably well with those derived from Q-band ENDOR (Table 1). The quadrupole coupling is similar to those observed in metal-coordinated imidazole nitrogens [88]. HYSCORE spectra were used to identify the pairs of resonances corresponding to each nitrogen nucleus [77,78]. In benzene dioxygenase [77] an additional resonance was assigned to a third ^{14}N coupling (Table 1), which was taken as evidence for a peptide nitrogen, as observed in the plant-type ferredoxins.

7. Pulsed ENDOR

Pulsed ENDOR methods which are now being used for metalloproteins are based on pulse sequences introduced by Mims [89] and Davies [90] A number of techniques have been developed and used for biological samples based on pulsed ENDOR [72,91–93]. These involve applying pulses of r.f. radiation during the spin-echo EPR sequence. In principle the spectra may be easier to obtain than c.w. ENDOR because there is no requirement for saturation of the EPR signal.

Fan et al. [63] used Mims pulsed ENDOR to detect ^{2}H coupling to iron–sulfur clusters, after exchange into $^{2}H_2O$. They applied this method to show the presence of hydrogen bonds to the [2Fe–2S] cluster in the plant-type ferredoxin from *Anabaena*.

A pulsed ENDOR spectrum is shown in Fig. 6, for the Rieske cluster in benzene dioxygenase. Coupling to ^{14}N and ^{1}H can be observed, although the latter are not as well resolved as in the first-derivative c.w. ENDOR spectra of Fig. 3. Other pulse sequences such as Davies ENDOR, which is more sensitive to stronger coupling may lead to improvements in resolution.

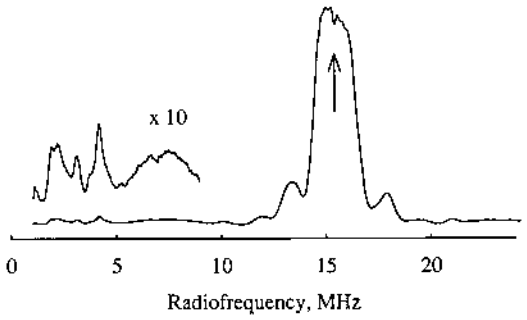

Fig. 6. Pulsed ENDOR spectrum of the Rieske cluster of benzene dioxygenase. The spectrum was recorded with a Mims ENDOR sequence, at a temperature of 7.5 K, at a magnetic field of 362 mT, corresponding to $g_2 = 1.877$. The arrow points to the proton larmor frequency (J. Shergill, S. Rigby, P. Höfer, unpublished results). The amplified region shows coupling to ^{14}N.

8. NMR

Although it is not the main topic of this review, mention should be made of the results from NMR spectroscopy. Contact shifts of protons in NMR contain structural information analogous to that available from ENDOR [14,94]. The two measurements are not directly comparable since solid-state ENDOR measured at liquid helium temperatures gives information on the ground states of the iron–sulfur clusters; oxidized [2Fe–2S] clusters are diamagnetic under these conditions. NMR is measured in solution at room temperature and therefore observes the paramagnetic excited states of the spin-coupled [2Fe–2S] cluster; it shows contact shifts in both the oxidized and reduced forms [57,94]. The advantage of the NMR method is that by tracing the chain of the protein it is possible to make sequence-specific assignments of contact-shifted resonances [11,95,96]. These become progressively more difficult in the vicinity of the paramagnetic centre owing to spin relaxation effects, but strategies are being developed to overcome these difficulties [10,97]. In this way it was possible to demonstrate that the ferrous atom of the reduced cluster in plant-type ferredoxins is the one closest to the surface [10].

NMR spectra have been taken of a Rieske-type ferredoxin from the alkene monooxygenase of *Xanthobacter* strain Py2 [98] For the reduced protein, well-resolved hyperfine-shifted resonances were observed in the $+90$ to -20 ppm range. Exchangeable protons were assigned to histidine ring protons. The others were assigned to α- and β-CH_2 resonances of cysteine or histidine.

9. Conclusions

Application of the EPR-based techniques ENDOR and ESEEM has highlighted the similarities and differences between the various types of [2Fe–2S] clusters in proteins. New types of structural information have been derived, such as the

imidazole coordination in the Rieske clusters, and the effects of exchange of protons with solvent. They make it possible to observe interactions with protons, which are not observed by X-ray crystallography. Each method has its strengths and limitations, and they are more powerful when correlations are made with other types of spectroscopy such as Mössbauer and resonance Raman. Correlations of hyperfine parameters with structural methods will make it possible to learn about chemical states which are inaccessible to crystallography and NMR, such as kinetic transient states which are trapped by freezing, or photolyzed states of proteins. ENDOR and pulsed EPR also show promise to identify changes in proteins induced by genetic engineering.

Acknowledgements

We are indebted to numerous collaborators with whose expertise made possible the various measurements presented, in particular Alan Chapman, David Duetschman, Jacques Meyer, Jeremy Mason, John McCracken, Jack Peisach, Krishna Rao, Steve Rigby and Andy White. EG is supported by a studentship from the Engineering and Physical Sciences Research Council.

References

[1] R. Cammack, Adv. Inorg. Chem. 38 (1992) 281.
[2] H. Beinert, R.H. Holm, E. Münck, Science 277 (1997) 653.
[3] M.K. Johnson, Curr. Opin. Chem. Biol. 2 (1998) 173.
[4] J.C.M. Tsibris, R.W. Woody, Coord. Chem. Rev. 5 (1970) 417.
[5] K. Fukuyama, N. Ueki, H. Nakamura, T. Tsukihara, H. Matsubara, J. Biochem. 117 (1995) 1017.
[6] A.K. Chamberlain, T.M. Handel, S. Marqusee, Nat. Struct. Biol. 3 (1996) 1055.
[7] A. Müller, J.J. Müller, Y.A. Müller, H. Uhlmann, R. Bernhardt, U. Heinemann, Structure 6 (1998) 269.
[8] B. Kauppi, K. Lee, E. Carredano, R.E. Parales, D.T. Gibson, H. Eklund, S. Ramaswamy, Structure 6 (1998) 571.
[9] H.M. Holden, B.L. Jacobson, J.K. Hurley, G. Tollin, B.H. Oh, L. Skjeldal, Y.K. Chae, H. Cheng, B. Xia, J.L. Markley, J. Bioenerg. Biomembr. 26 (1994) 67.
[10] L.B. Dugad, G.N. Lamar, L. Banci, I. Bertini, Biochemistry 29 (1990) 2263.
[11] H. Cheng, W.M. Westler, B. Xia, B.H. Oh, J.L. Markley, Arch. Biochem. Biophys. 316 (1995) 619.
[12] T.C. Pochapsky, X.M. Ye, G. Ratnaswamy, T.A. Lyons, Biochemistry 33 (1994) 6424.
[13] H. Cheng, J.L. Markley, Ann. Rev. Biophys. Biomol. Struct. 24 (1995) 209.
[14] I. Bertini, S. Ciurli, C. Luchinat, Struct. Bonding 83 (1995) 1.
[15] M.T. Werth, H. Sices, G. Cecchini, I. Schroder, S. Lasage, R.P. Gunsalus, M.K. Johnson, FEBS Lett. 299 (1992) 1.
[16] J.M. Moulis, V. Davasse, M.P. Golinelli, J. Meyer, I. Quinkal, J. Biol. Inorg. Chem. 1 (1996) 2.
[17] M.T. Werth, G. Cecchini, A. Manodori, B.A.C. Ackrell, I. Schroder, R.P. Gunsalus, M.K. Johnson, Proc. Natl. Acad. Sci. USA 87 (1990) 8965.
[18] L.E. Mortenson, R.C. Valentine, J.E. Carnahan, Biochem. Biophys. Res. Commun. 7 (1962) 448.
[19] K. Tagawa, D.I. Arnon, Nature 195 (1962) 537.
[20] C.C. Correll, M.L. Ludwig, C.M. Bruns, P.A. Karplus, Protein Sci. 2 (1993) 2112.
[21] M.G. Darlison, J.R. Guest, Biochem. J. 223 (1984) 507.

[22] D. Wood, M.G. Darlison, R.J. Wilde, J.R. Guest, Biochem. J. 222 (1984) 519.
[23] R. Hille, W.R. Hagen, W.R. Dunham, J. Biol. Chem. 260 (1985) 10569.
[24] M.J. Romao, M. Archer, I. Moura, J.J.G. Moura, J. Legall, R. Engh, M. Schneider, P. Hof, R. Huber, Science 270 (1995) 1170.
[25] R.W.F. Hardy, F. Knight, C.C. McDonald, A.S. D'Eustacio, in: A. San Pietro (Ed.), Nonheme iron proteins, role in energy conversion, Antioch Press, Yellow Springs, OH, 1965, p. 275.
[26] J. Cardenas, L.E. Mortenson, D.C. Yoch, Biochim. Biophys. Acta 434 (1976) 244.
[27] J. Meyer, M. Bruschi, J.J. Bonicel, G.E. Bovier–Lapierre, Biochemistry 25 (1986) 6054.
[28] J. Meyer, J.M. Moulis, M. Lutz, Biochem. Biophys. Res. Commun. 119 (1984) 828.
[29] J.K. Shergill, M.P. Golinelli, R. Cammack, J. Meyer, Biochemistry 35 (1996) 12842.
[30] J.S. Rieske, R.E. Hansen, W.S. Zaugg, J. Biol. Chem. 239 (1964) 3017.
[31] R.J. Gurbiel, C.J. Batie, M. Sivaraja, A.E. True, J.A. Fee, B.M. Hoffman, D.P. Ballou, Biochemistry 28 (1989) 4861.
[32] R.J. Gurbiel, T. Ohnishi, D.E. Robertson, F. Daldal, B.M. Hoffman, Biochemistry 30 (1991) 11579.
[33] R.D. Britt, K. Sauer, M.P. Klein, D.B. Knaff, A. Kriauciunas, C.A. Yu, L. Yu, R. Malkin, Biochemistry 30 (1991) 1892.
[34] S. Iwata, M. Saynovits, T.A. Link, H. Michel, Structure 4 (1996) 567.
[35] C.S. Butler, J.R. Mason, Adv. Microbial Physiol. 38 (1997) 47.
[36] J.F. Cline, B.M. Hoffman, W.B. Mims, E. LaHaie, D.P. Ballou, J.A. Fee, J. Biol. Chem. 260 (1985) 3251.
[37] J.R. Mason, R. Cammack, Annu. Rev. Microbiol. 46 (1992) 277.
[38] J. Meyer, J.M. Moulis, M. Lutz, Biochim. Biophys. Acta 871 (1986) 243.
[39] J. Fritz, R. Anderson, J. Fee, G. Palmer, R.H. Sands, W.H. Orme–Johnson, H. Beinert, J.C.M. Tsibris, I. Gunsalus, Biochim Biophys Acta 253 (1971) 110.
[40] W.R. Hagen, J. Magn. Reson. 44 (1981) 447.
[41] G. Feher, in: G.R. Eaton, S.S. Eaton, K.M. Sakhilov (Eds.), Foundations of Modern EPR, World Scientific, Singapore, 1988, pp. 548–556.
[42] J. Hüttermann, R. Kappl, in: H. Sigel (Ed.), Metal ions in Biological Systems: ENDOR, EPR and Electron Spin Echo for Probing Coordination Spheres, vol. 22, Marcel Dekker, New York, 1987, pp. 1–80.
[43] J. Hüttermann, in: L.J. Berliner, J. Reuben (Eds.), EMR of paramagnetic molecules, vol. 13, Plenum Press, New York, 1993, pp. 219–252.
[44] J. Hüttermann, in: M.C.R. Symons (Ed.), Specialist periodical reports: Electron spin resonance, vol. 15, Royal Society of Chemistry, London, 1996, pp. 59–111.
[45] B.M. Hoffman, Accounts Chem. Res. 24 (1991) 164.
[46] D.J. Lowe, ENDOR and EPR of Metalloproteins, Springer, Berlin, 1995.
[47] J.H. Rist, J.S. Hyde, J. Chem. Phys. 52 (1970) 4633.
[48] T.A. Henderson, G.C. Hurst, R.W. Kreilick, J. Am. Chem. Soc. 107 (1985) 7299.
[49] B.M. Hoffman, J. Martinsen, R.A. Venters, J. Magn. Reson 62 (1985) 537.
[50] B.M. Hoffman, R.J. Gurbiel, J. Magn. Reson. 82 (1989) 309.
[51] J. Hüttermann, G.P. Däges, H. Reinhard, G. Schmidt, in: G. La Mar (Ed.), Nuclear Magnetic Resonance of Paramagnetic Molecules, Kluwer, The Netherlands, 1995, pp. 165–192.
[52] C.J. Bender, P. Aisen, Methods Enzymol. 227 (1973) 190.
[53] W.R. Dunham, G. Palmer, R.H. Sands, A.J. Bearden, Biochim. Biophys. Acta 253 (1971) 373.
[54] W.R. Dunham, A.J. Bearden, I.T. Salmeen, G. Palmer, R.H. Sands, W.H. Orme-Johnson, H. Beinert, Biochim. Biophys. Acta 253 (1971) 134.
[55] K.K. Rao, R. Cammack, D.O. Hall, C.E. Johnson, Biochem. J. 122 (1971) 257.
[56] G. Palmer, W.R. Dunham, J.A. Fee, R.H. Sands, T. Iizuka, T. Yonetani, Biochim. Biophys. Acta 245 (1971) 201.
[57] M. Poe, W.D. Phillip, C.C. McDonald, W. Lovenberg, Proc. Natl. Acad. Sci. USA 68 (1971) 68.
[58] J.F. Gibson, D.O. Hall, J.H.M. Thornley, F.R. Whatley, Proc. Natl. Acad. Sci. USA 56 (1966) 987.
[59] J.H. Thornley, J.F. Gibson, F.R. Whatley, D.O. Hall, Biochem. Biophys. Res. Commun. 24 (1966) 877.
[60] M. Bowman, L. Kevan, K. Mukai, T. Kimura, Biochim. Biophys. Acta 328 (1973) 244.

[61] R.E. Anderson, W.R. Dunham, R.H. Sands, A.J. Bearden, H.L. Crespi, Biochim. Biophys. Acta 408 (1975) 306.
[62] N.R. Orme-Johnson, W.B. Mims, W.H. Orme-Johnson, R.G. Bartsch, M.A. Cusanovich, J. Peisach, Biochim. Biophys. Acta 748 (1983) 68.
[63] C.L. Fan, M.C. Kennedy, H. Beinert, B.M. Hoffman, J. Am. Chem. Soc. 114 (1992) 374.
[64] J.K. Shergill, R. Cammack, Biochim. Biophys. Acta 1185 (1994) 35.
[65] A. Riedel, S. Fetzner, M. Rampp, F. Lingens, U. Liebl, J.L. Zimmermann, W. Nitschke, J. Biol. Chem. 270 (1995) 30869.
[66] J.K. Shergill, R. Cammack, Biochim. Biophys. Acta 1185 (1994) 43.
[67] R.J. Gurbiel, P.E. Doan, G.T. Gassner, T.J. Macke, D.A. Case, T. Ohnishi, J.A. Fee, D.P. Ballou, B.M. Hoffman, Biochemistry 35 (1996) 7834.
[68] A.L.P. Houseman, B.H. Oh, M.C. Kennedy, C.L. Fan, M.M. Werst, H. Beinert, J.L. Markley, B.M. Hoffman, Biochemistry 31 (1992) 2073.
[69] W.B. Mims, Phys. Rev. B 5 (1972) 2409–2419.
[70] W.B. Mims, J. Peisach, in: A.J. Hoff (Ed.), Advanced EPR: Applications in Biology and Biochemistry, Elsevier, Amsterdam, 1989, pp. 1–57.
[71] S.A. Dikanov, Y.D. Tsvetkov, Electron Spin Echo Envelope Modulation (ESEEM) Spectroscopy, CRC Press, Boca Raton, 1992.
[72] D. Goldfarb, in: M.C.R. Symons (Ed.), Specialist Periodical Reports: Electron Spin Resonance, vol. 15, Royal Society of Chemistry, London, 1996, pp. 186–243.
[73] H.L. Flanagan, D.J. Singel, J. Chem. Phys. 87 (1987) 5606.
[74] E.J. Reijerse, C.P. Keijzers, J. Magn. Reson. 71 (1987) 83.
[75] R.D. Britt, J.L. Zimmermann, K. Sauer, M.P. Klein, J. Am. Chem. Soc. 111 (1989) 3522.
[76] (a) J.J. Shane, P.A.A. van der Heijden, E.J. Reijerse, E. de Boer, Appl. Mag. Res. 6 (1994) 427. (b) P. Höfer, Bruker Report 118 (1991) 1.
[77] J.K. Shergill, C.L. Joannou, J.R. Mason, R. Cammack, Biochemistry 34 (1995) 16533.
[78] S.A. Dikanov, L.Y. Xun, A.B. Karpiel, A.M. Tyryshkin, M.K. Bowman, J. Am. Chem. Soc. 118 (1996) 8408.
[79] J. Peisach, N.R. Orme-Johnson, W.B. Mims, W.H. Orme-Johnson, J. Biol. Chem. 252 (1977) 5643.
[80] S.A. Dikanov, M.K. Bowman, J. Biol. Inorg. Chem. 3 (1998) 18.
[81] M.J. Hunt, A.L. Mackay, J. Magn. Reson. 22 (1976) 295.
[82] M. vanGastel, J.W.A. Coremans, L.J.C. Jeuken, G.W. Canters, E.J.J. Groenen, J. Phys. Chem. A 24 (1998) 4462.
[83] R. Cammack, A. Chapman, J. McCracken, J.B. Cornelius, J. Peisach, J.H. Weiner, Biochim. Biophys. Acta 956 (1988) 307.
[84] S.A. Dikanov, A.M. Tyryshkin, I. Felli, E.J. Reijerse, J. Hüttermann, J. Magn. Reson. B 108 (1995) 99.
[85] A. Chapman, R. Cammack, D.J. Linstead, D. Lloyd, Eur. J. Biochem. 156 (1986) 193.
[86] H.Y. Liu, J.P. Germanas, J. Inorg. Biochem. 72 (1998) 127.
[87] R. Cammack, A. Chapman, J. Peisach, J. McCracken, J. Chem. Soc. Faraday Trans. 87 (1991) 3203.
[88] C.I. Ashby, C.P. Cheng, T.L. Brown, J. Am. Chem. Soc. 100 (1978) 6057.
[89] W.B. Mims, Proc. Roy. Soc. A. 283 (1965) 452.
[90] E.R. Davies, Phys. Lett. A 47 (1974) 1.
[91] H. Thomann, M. Bernardo, in: L.J. Berliner, J. Reuben (Eds.), EMR of Paramagnetic Molecules, vol. 13, Plenum Press, New York, 1993, pp. 275–322.
[92] A. Schweiger, Angew. Chem. 30 (1991) 265.
[93] B.M. Hoffman, V. DeRose, P.E. Doan, R.J. Gurbiel, A.L.P. Houseman, J. Telser, in: L.J. Berliner, J. Reuben (Eds.), EMR of Paramagnetic Molecules, vol. 13, Plenum Press, New York, 1993, pp. 151–218.
[94] L. Banci, I. Bertini, C. Luchinat, Struct. Bonding 72 (1990) 113.
[95] Y.K. Chae, F. Abildgaard, E.S. Mooberry, J.L. Markley, Biochemistry 33 (1994) 3287.
[96] C. Lelong, P. Setif, H. Bottin, F. Andre, J.M. Neumann, Biochemistry 34 (1995) 14462.
[97] L. Skjeldal, W.M. Westler, B.H. Oh, A.M. Krezel, H.M. Holden, B.L. Jacobson, I. Rayment, J.L. Markley, Biochemistry 30 (1991) 7363.
[98] R.C. Holz, F.J. Small, S.A. Ensign, Biochemistry 36 (1997) 14690.
[99] J.K. Shergill, Ph.D. thesis: University of London, 1993.